

# State-independent robust heat-bath algorithmic cooling of nuclear spins

Krishna Shende,<sup>1,\*</sup> Arvind,<sup>1,2,†</sup> and Kavita Dorai<sup>1,‡</sup>

<sup>1</sup>*Department of Physical Sciences, Indian Institute of Science Education & Research Mohali, Sector 81 SAS Nagar, Manauli PO 140306 Punjab India.*

<sup>2</sup>*Punjabi University Patiala, 147002, Punjab, India*

In this work, we experimentally demonstrate the implementation of a recently proposed robust and state-independent heat-bath algorithmic cooling (HBAC) method [1] on an NMR quantum processor. While HBAC methods improve the purity of a quantum system via iterative unitary entropy compression, they are difficult to implement experimentally since they use sort operations that are different for each iteration. The new robust HBAC method proved that optimal HBAC is possible without prior state information and using a single fixed operation. We modified the protocol to experimentally perform efficient cooling of <sup>13</sup>C and <sup>15</sup>N spins and provide an optimal decomposition of this modified protocol in terms of quantum gates. This is the first time that optimal HBAC has been experimentally demonstrated on <sup>15</sup>N spins. We examined the relaxation dynamics of these algorithmically cooled spins, in order to ascertain the effect of decoherence on the cooled states.

## I. INTRODUCTION

Quantum computers have the potential to increase the speed and efficiency of certain computational algorithms and simulations [2–4]. However, physical realizations of quantum computers have proved challenging, since sensitive quantum mechanical effects are easily overwhelmed by thermal fluctuations, and small errors during the implementation of quantum operations are detrimental to their efficient implementation [5]. Protocols such as quantum error correction and fault tolerant computation were developed to curb these errors, which require the supply of pure qubits throughout the computation process [6].

NMR quantum processors use ensembles of nuclear spins to perform quantum computational tasks and have the advantages of long qubit decoherence times and optimal gate implementation via high-precision rf pulses [7–9]. Nuclear spins at room temperature are in Boltzmann equilibrium, and thus this highly mixed ensemble leads to a major disadvantage for quantum computation which requires highly pure ensembles [10]. The NMR quantum information processor has been termed as a system having ‘good dynamics versus bad kinematics’ [11]. To improve this situation, we need to prepare the initial state of the NMR quantum information processor such that a large number of spins in the ensemble are in the same quantum state. One way to prepare an ensemble of spins in a pure state is to cool the entire system down to very low temperatures, which however is not feasible with the current technology. Other spin-cooling proposals include algorithmic cooling [12], dynamic nuclear polarization [13], parahydrogen induced polarization [14] and optical pumping [15], all of which have met with varying degrees of success.

The population difference between the  $|0\rangle$  and  $|1\rangle$  of an NMR qubit is termed as the ‘spin polarization ( $\epsilon$ )’ and at thermal equilibrium:

$$\epsilon = P_{|0\rangle} - P_{|1\rangle} = \tanh\left(\frac{\Delta E}{2k_B T}\right) \approx \frac{\hbar\gamma B_z}{2k_B T} \quad (1)$$

where  $\gamma$  is the gyromagnetic ratio,  $B_z$  is the intensity of the external Zeeman magnetic field,  $k_B$  is the Boltzmann constant,  $T$  is the temperature of the bath, and  $\Delta E \ll k_B T$ . The spin temperature is defined as  $T_{\text{spin}} = \frac{\hbar\gamma B_z}{2k_B \epsilon}$  and spins with a polarization higher than their room temperature polarization, can be considered to be ‘cooled down’. Cooling of nuclear spins is hence equivalent to increasing their polarization which is limited by the Shannon bound [16].

The method for increasing polarization of selected qubits in a closed system was introduced by Schulman [12] and is known as algorithmic cooling (AC). Here, additional ancilla qubits are required which are called reset qubits, and the combined system qubits and reset qubits are subjected to an overall unitary transformation such that the system qubits move towards a state with lower entropy/increased purity and hence with a lower spin temperature, while the reset qubits heat up and gain entropy. The major disadvantage of the AC protocol is that for spins at room temperature, the number of spins required to cool the target spin is very large (typically  $\approx 10^{12}$  spins). This obstacle was circumvented by Boykin [17] in an extension to AC called heat-bath algorithmic cooling (HBAC), wherein a contact between the heat bath and the system is introduced, which pumps the excess entropy out of the system into this heat bath [18, 19]. Later an extension to the HBAC method was proposed, the partner pairing algorithm (PPA), which sorts the diagonal elements of a density matrix for entropy compression, and it was proved that this sort operation is an optimal entropy compression step for HBAC [20]. If the decoherence time of the reset qubits is significantly smaller than that of the computational qubits, it is possible to iteratively achieve cool-

\* ph19032@iisermohali.ac.in

† arvind@iisermohali.ac.in

‡ kavita@iisermohali.ac.in

ing of the target qubits. However, despite repetitive cooling, the target qubits cannot be fully purified, and a limit of purification has been computed [21–23]. The role of non-Markovian processes in improving cooling efficiency was explored and several protocols were suggested to optimize the thermalization strategy [24]. It was discovered that the unitarity of the compression operation is what limits the cooling of HBAC techniques [25]. It was recently demonstrated that the cooling limit of HBAC protocols can be enhanced in the presence of noise [26]. The overall methodology of all these methods is to perform various unitary transformations on a multi-spin system where part of the system moves towards a higher polarization, lower entropy and hence lower effective spin temperature, at the cost of the other part which heats up, and in some of the methods this heat is transported away by another set of transformations.

On NMR quantum processors, various experiments based on the HBAC protocol have been performed [27–32], some of which showed polarization enhancement beyond Shannon’s limit. Several iterations of HBAC was performed on three solid-state NMR qubits in order to cool a single qubit [33]. The PPA-HBAC algorithm was used to implement a quantum Otto heat engine with greater thermal efficiency beyond traditional engines [34]. An HBAC method using correlated spin-bath interactions was devised which uses spin-spin cross-relaxation (the nuclear Overhauser effect) to achieve higher polarization enhancement as compared to the PPA-HBAC method [35]. Recently, HBAC has been used to enhance spin polarization in NV center quantum devices [36].

All the previous experimental implementations of HBAC achieved cooling via the PPA-HBAC method, which requires a different compression unitary to be implemented as well as knowledge of the state of the system in every iteration. The work done in this paper is a realization of Raesi’s state-independent HBAC technique [1] on an NMR quantum processor, which proposed a new fixed operation to achieve algorithmic cooling that does not require any prior knowledge of the state. We experimentally demonstrate the successful implementation of this new protocol on two different three-qubit NMR systems: the first system having a  $^{13}\text{C}$  spin as the target qubit to be cooled and the second system having a  $^{15}\text{N}$  spin as the target qubit to be cooled. We were able to achieve large polarization enhancements and concomitantly were able to decrease the corresponding spin temperatures of the target spins to well below room temperature. The original theoretical proposal decomposed the fixed unitary compression operator in terms of shift operators, which were further decomposed in terms of the quantum Fourier transform (QFT), the inverse QFT, and single-qubit rotation gates. The QFT is a resource-intensive operation whose circuit depth increases tremendously with the number of qubits, which makes it more vulnerable to experimental errors [37]. We hence designed an optimal decomposition of the shift operators in terms of standard multiqubit gates such as Toffoli,

CNOT and NOT gates, which makes it easier to experimentally implement the circuit. After implementing several cycles of TSAC cooling, We were able to enhance the polarization of the  $^{13}\text{C}$  and  $^{15}\text{N}$  spins by 4.3 and 5.95 times respectively, as compared to their thermal equilibrium polarizations, which translates to cooling their spin temperatures down to  $\approx 71\text{ K}$  and  $\approx 51\text{ K}$ , respectively. It is noteworthy that  $^{15}\text{N}$  spins (due to their low gyromagnetic ratio) have very low spin polarizations at thermal equilibrium ( $\approx 1/10$ th that of  $^1\text{H}$  spins), and we were able to considerably enhance their polarization via the state-independent HBAC protocol. This is the first experiment that demonstrates cooling of  $^{15}\text{N}$  spins using HBAC methods. Further, we studied the relaxation dynamics of the algorithmically cooled spins by measuring their  $T_1$  and  $T_2$  relaxation rates and observed that algorithmically cooled states relax in a way similar to thermal states, thus retaining the good dynamics of the NMR spin system.

This paper is organized as follows: The standard HBAC and PPA-HBAC protocols are described in Section II A, while the new state-independent TSAC protocol is given in Section II B. The optimal circuit decomposition of the compression unitary is described in Section II C. The experimental implementation of the new state-independent HBAC protocol is presented in Section III. Section III A contains experimental details, while Sections III B and III C describe the results of experimentally cooling a  $^{13}\text{C}$ -labeled system and a  $^{13}\text{C}$ - $^{15}\text{N}$ -labeled system, respectively. Section IV contains a few concluding remarks.

## II. THEORETICAL FRAMEWORK

### A. Standard Heat-Bath Algorithmic Cooling Protocols

The AC scheme exploits the fact that cooling of specific spins below their equilibrium polarization can be achieved by using a reversible unitary operation to increase the polarization of the target spins, relative to the rest of the spins. Closed system AC executes an entropy compression operation on spins which are initially at thermal equilibrium which creates a difference in the spin temperatures of the spins such that, the reset spins heat up and the computational spins cool down, as represented by [12]:

$$\rho_{\epsilon_i}^{\otimes n} = \rho \xrightarrow{\text{compression}} \rho' = U\rho U^\dagger = \rho_{\epsilon_c} \otimes \rho_{\epsilon_r}^{\otimes n-1} \quad (2)$$

where  $\epsilon_i$  is the initial polarization, and  $\epsilon_c$  and  $\epsilon_r$  are the polarizations of the computational spin and reset spin respectively,  $\epsilon_c > \epsilon_i > \epsilon_r$  after entropy compression.

The density matrix of the computational spin is obtained by taking a trace over the  $n - 1$  reset spin ( $\rho_{\epsilon_c} = \text{Tr}_{n-1}(\rho')$ ). A major disadvantage of the AC method is the fact that cooling is limited by the Shannon bound for information compression [16, 38].

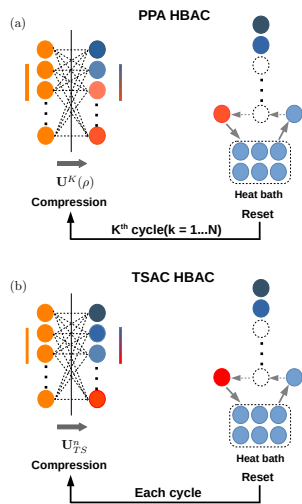


FIG. 1. Schematic to illustrate the different steps of the PPA-HBAC and state-independent HBAC protocols. The  $n$  spin system is categorized into target spins and reset spins. Temperature is color coded, with shades of blue indicating cooling and shades of orange indicating heating. (a) During every iteration in the PPA HBAC method, the compression unitary  $U^1 U^2 \dots U^K \dots U^N$  extracts entropy from the target spin and redistributes it among the reset spins, such that the target spin cools down and the reset spins heat up. The compression step is followed by a reset step, where the hot reset spins are brought into contact with the heat-bath. The compression unitary  $U^K(\rho)$  depends on the state  $\rho$  and changes after every cooling cycle, where  $K = 1, 2, \dots, N$  and  $N$  denotes the maximum number of cooling cycles implemented. (b) Only a fixed compression unitary  $U_{TS}^n$  is required in the state-independent TSAC HBAC method to redistribute entropy and develop a temperature gradient among spins. The compression step is followed by a reset step where the reset spins equilibrate with the surrounding heat-bath. The dotted lines in (a) and (b) indicate redistribution of entropy among the system spins to create a temperature gradient.

Cooling in the AC scheme can be enhanced by incorporating a contact between a heat bath and the system. The excessive heat in the reset spins is then pumped out of the system into a heat bath, where it is removed and the spins are cooled to the bath temperature a step called the 'reset' step [17]. The system spins are categorized as a target spin (which is to be cooled), a set of scratch spins (which can either be a higher-dimensional qudit or a string of qubits) which help in entropy compression, and a set of  $m$  reset spins which are brought into contact with the heat-bath [23]. The target and scratch spins together are referred to as the computational spins. The entire process of entropy compression and the reset step is known as heat bath algorithmic cooling (HBAC)[18][19]. The HBAC method works optimally if the ratio  $R$  between the thermalization times ( $T_1$ ) of computational to reset spins satisfies  $R \gg 1$ , so that several cooling cycles can be implemented, and the state of the computational spins remains unchanged during the reset process. The

reset step amounts to tracing over the reset spins and replacing them with heat-bath spins. It is assumed that the heat-bath capacity is so large that the spin-bath interaction has no effect on the bath temperature.

The HBAC method was further optimized in a method called the partner pairing(PPA) algorithm [20], where in each iteration the diagonal elements of the density matrix are sorted in decreasing order. It is to be noted that the sort operations and their complexity keep changing from iteration to iteration.

The steps of the PPA HBAC algorithm can be written as:

$$\begin{aligned} \rho &\xrightarrow{C} \rho' = U_C \rho U_C^\dagger \\ \rho' &\xrightarrow{S} \rho'' = U_S(\rho') \rho' U_S^\dagger(\rho') \\ \rho'' &\xrightarrow{R} \rho''' = \text{Tr}_m [\mathcal{L}(\rho'' \otimes \rho_{\epsilon_b}^{\otimes m})] \end{aligned} \quad (3)$$

Here  $U_C$  and  $U_S$  are unitaries involved in compression and sorting steps and act on the system qubits, while  $\mathcal{L}$  represents non-unitary evolution during the period in which the reset qubits cool down due to interaction with the heat bath;  $\rho_{\epsilon_b}$  represents the state of the bath spin and  $\epsilon_b$  is the heat-bath polarization. The cooling limit is achieved once no more entropy extraction is possible i.e. when system state reaches a steady state which is not changed by compression and refresh ( $\rho = \rho'''$  in Eq. (3)) For  $n$  spins the PPA HBAC cooling limit i.e. the maximum achievable polarization is computed as [35]:

$$\epsilon_{\max} = \frac{(1 + \epsilon_b)^{2^{n-2}} - (1 - \epsilon_b)^{2^{n-2}}}{(1 + \epsilon_b)^{2^{n-2}} + (1 - \epsilon_b)^{2^{n-2}}} \quad (4)$$

Spin temperature is inversely proportional to the polarization and can be computed from:

$$T_1 \cdot \epsilon_1 = T_2 \cdot \epsilon_2 \quad (5)$$

where  $T_1, T_2$  are the initial and final spin temperatures and  $\epsilon_1, \epsilon_2$  are the initial and final spin polarizations, respectively.

An upper bound on spin cooling (i.e. on polarization enhancement), also called the *Shannon bound*, can be derived by interpreting the spin state in terms of information theory, wherein the information content (*IC*) of the spin is defined using Shannon entropy  $H$ , and the relation between spin polarization ( $\epsilon$ ) and *IC* is given by [23]:

$$\begin{aligned} H_{1qubit} &= \left[ \frac{1 - \epsilon}{2} \ln \left( \frac{1 - \epsilon}{2} \right) + \frac{1 + \epsilon}{2} \ln \left( \frac{1 + \epsilon}{2} \right) \right] \\ IC_{1qubit} &= 1 - H_{1qubit} = \frac{\epsilon^2}{\ln 4} + O(\epsilon^4). \end{aligned} \quad (6)$$

A major limitation of the PPA algorithm is that in each iteration, complete information about the state of the system is needed in order to set up the sort operation. In a domino effect, this in turn implies that the PPA compression operation also changes after every iteration, which makes PPA HBAC method experimentally challenging to implement.



compress entropy among spins, thereby creating a temperature gradient between the system spins. The target spin is cooled while the reset spins are heated up. The reset step is the same for the PPA HBAC and the TSAC HBAC protocols. The reset step is repeated several times to thermalize the reset spins to the heat-bath temperature.

### C. Optimal Circuit Decomposition of the Compression Unitary

The first and last operations of the  $U_{TS}$  unitary operator (the  $1 \times 1$  blocks in the top left and bottom right corners of the matrix) in Eq. (7) correspond to  $\text{SHIFT}_m$  operators which shift the spin state  $m$  times to the right or the left. This can be achieved by applying a multiple-control-Toffoli gate (which is a controlled-controlled-NOT with one target and  $n - 1$  controls) followed by a NOT gate on the last spin. The suggested decomposition in Raeisi et. al. [1] for these  $\text{SHIFT}$  operators is a QFT and an inverse QFT, sandwiching a set of rotation operators of specific rotation angles and phases.

In order to use fewer experimental resources and alleviate the detrimental effects of noise during long gate implementation times, we have decomposed the  $\text{SHIFT}$  operator into a sequence of a three-qubit Toffoli gate, a two-qubit CNOT gate and a single-qubit NOT gate. The complexity of the circuit has been further reduced by using an approximate Toffoli gate as described in Ref. [39], which differs from the actual Toffoli gate by a phase of one of its amplitudes (the phase of the  $|101\rangle$  state is reversed). The final compression unitary operator which has been experimentally implemented is given by:

$$U'_{TS} = \begin{bmatrix} 1 & 0 & 0 & 0 & 0 & 0 & 0 & 0 \\ 0 & 0 & 1 & 0 & 0 & 0 & 0 & 0 \\ 0 & 1 & 0 & 0 & 0 & 0 & 0 & 0 \\ 0 & 0 & 0 & 0 & 1 & 0 & 0 & 0 \\ 0 & 0 & 0 & 1 & 0 & 0 & 0 & 0 \\ 0 & 0 & 0 & 0 & 0 & 0 & -1 & 0 \\ 0 & 0 & 0 & 0 & 0 & 0 & 1 & 0 \\ 0 & 0 & 0 & 0 & 0 & 0 & 0 & 1 \end{bmatrix} \quad (9)$$

The negative sign at the  $|101\rangle\langle 110|$  position in the  $U'_{TS}$  unitary operator (Eq. (9)) has no effect on the TSAC protocol and the results remain the same.

The complete quantum circuit for implementing the TSAC protocol is depicted in Fig. 2(a), for a three-qubit system initially prepared in a thermal equilibrium state. The circuit inside the green box is the general compression unitary  $U'_{TS}$ , as given in Eq. (9). This unitary is decomposed as a sequence of a right  $\text{SHIFT}$  operator, a left  $\text{SHIFT}$  operator, a Toffoli gate and a NOT gate, enclosed in the blue dashed box, the red dashed box, the magenta shaded and the unfilled box, respectively, in Fig. 2(a). Each  $\text{SHIFT}$  operator is further decomposed as a Toffoli gate, a CNOT gate and a NOT gate given in the orange shaded, yellow shaded and unfilled boxes,

respectively. The reset step of the TSAC algorithm is denoted by the indigo shaded box, with the horizontal lines depicting the heat bath. Figs. 2(b)-(e) depict the NMR pulse sequences for a NOT, a CNOT and a Toffoli gate, respectively.

## III. EXPERIMENTAL IMPLEMENTATION

### A. Experimental details

All experiments were performed at ambient temperature (303 K) on a Bruker Avance III 600-MHz NMR spectrometer equipped with a standard 5 mm TXI probe. The Hamiltonian for a three-spin system in the rotating frame, assuming a high-temperature and high-field approximation, is given by [40]:

$$\mathcal{H} = -\hbar \sum_{i=1}^3 \omega_i I_z^i + \hbar \sum_{i<j=1}^3 J_{ij} I_z^i I_z^j \quad (10)$$

where  $\omega_i, I_z^i$  represent the offset frequency and the  $z$ -component of the spin angular momentum of the  $i$ th spin respectively, and  $J_{ij}$  is the strength of the scalar coupling between the  $i$ th and  $j$ th spins.

The TSAC cooling protocol was experimentally implemented on two molecules. The first molecule was  $^{13}\text{C}_2$ -labeled glycine with the spin denoted as  $^{13}\text{C}1$  being the target spin to be cooled and the  $^1\text{H}$  spin being the reset spin (see Fig. 4(a) for the molecular structure, chemical shifts  $\nu_i$  and  $J_{ij}$  scalar coupling values). The glycine molecule was dissolved in  $\text{D}_2\text{O}$  and a paramagnetic reagent  $\text{Cr}(\text{acac})_3$  was added to improve the  $T_1$  ratio between the target and reset nuclei. This molecule is an example of an  $\text{A}_2\text{XX}'$  spin system, with two equivalent  $^1\text{H}$  spins ( $\text{A}_2$ ) and two magnetically inequivalent  $^{13}\text{C}$  spins ( $\text{XX}'$ ). The second molecule was  $^{13}\text{C}$ - $^{15}\text{N}$ -labeled formamide, with both the  $^{15}\text{N}$  and the  $^{13}\text{C}$  spins being the targets to be cooled, and the  $^1\text{H}$  spin being the reset spin (see Fig. 7(a) for the molecular structure, chemical shifts  $\nu_i$  and  $J_{ij}$  scalar coupling values). Each single-qubit rotation gate was implemented using spin-selective rf pulses of appropriate phase, power and time duration, while two-qubit and three-qubit gates were implemented via evolution under the system Hamiltonian using time delays interspersed with  $\pi$  pulses to refocus chemical shifts and retain only the desired scalar coupling interactions. More experimental details of NMR pulse sequences for various quantum gates used in this work can be found in References [41–43]. On the TXI probe, the duration of the  $\frac{\pi}{2}$  pulses for  $^{15}\text{N}$ ,  $^{13}\text{C}$  and  $^1\text{H}$  were 38  $\mu\text{s}$  at a power level of 246.6 W, 12.95  $\mu\text{s}$  at a power level of 237.3 W, and 7.3  $\mu\text{s}$  at a power level of 19.9 W, respectively. Gradient ascent pulse engineering (GRAPE), an optimal control algorithm, was used to generate high-fidelity rf pulses of duration  $\approx 150\mu\text{s}$  to implement single-qubit rotations on the  $^{13}\text{C}_2$ -labeled glycine system. The total time taken to implement the

compression unitary on the  $^{13}\text{C}_2$ -labeled glycine system and on the  $^{13}\text{C}$ - $^{15}\text{N}$ -labeled formamide system was 0.302 s and 0.23 s respectively, which is much shorter than the relaxation times of all the spins in both systems.

### B. Experimentally Cooling the $^{13}\text{C}$ Spin

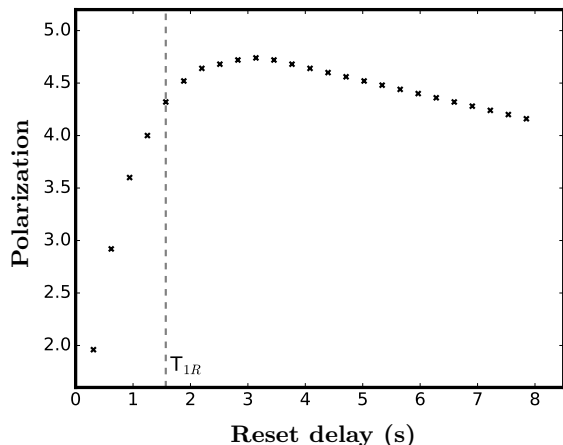


FIG. 3. Simulation of  $^{13}\text{C}1$  spin polarization as a function of the TSAC reset delay for the  $^{13}\text{C}_2$ -labeled glycine system;  $T_{1R}$  marks the  $T_1$  relaxation time of the  $^1\text{H}$  reset spin.

Most previous experimental algorithmic cooling protocols have focused on cooling  $^{13}\text{C}$  spins, due to their small gyromagnetic ratios and correspondingly low initial polarization at thermal equilibrium ( $\approx 1/4$ th that of the  $^1\text{H}$  spin). We hence chose  $^{13}\text{C}1$  as the target spin to be cooled in the  $^{13}\text{C}_2$ -labeled glycine system and the  $^1\text{H}$  spin as the reset spin due to its high polarization (set to 1.0) at thermal equilibrium and its fast  $T_1$  relaxation time as compared to the  $^{13}\text{C}1$  spin. Interestingly, this system has another  $^{13}\text{C}2$  spin, whose polarization also has the potential to be enhanced. However, as will be seen below, due to its unfavorable relaxation properties this spin does not cool down to the same extent as the target spin.

#### Optimizing the TSAC reset delay:

We simulated the change in  $^{13}\text{C}1$  spin polarization as a function of the reset delay in order to find the optimum reset delay for iterative TSAC cooling. We assumed ideal compression gate implementation and accounted for the decay in the polarization during the reset delay which is governed by:

$$\epsilon_t = (\epsilon_{\text{init}} - \epsilon_{\text{eq}}) \exp^{-t/T_1} + \epsilon_{\text{eq}} \quad (11)$$

where  $\epsilon_{\text{init}}$  and  $\epsilon_{\text{eq}}$  are the initial and thermal equilibrium spin polarizations, respectively. The reset delay was varied from  $0.2 \cdot T_{1R}$  to  $5 \cdot T_{1R}$ , where  $T_{1R}$  is the longitudinal relaxation time of the reset qubit, and as can be seen from Fig. 3, maximum  $^{13}\text{C}1$  polarization was obtained

for a reset delay of 3.14 s, which is  $\approx 2T_{1R}$ . We hence set the reset delay time during heat-bath interaction to this optimal value in our experiments and performed multiple rounds of TSAC cooling.

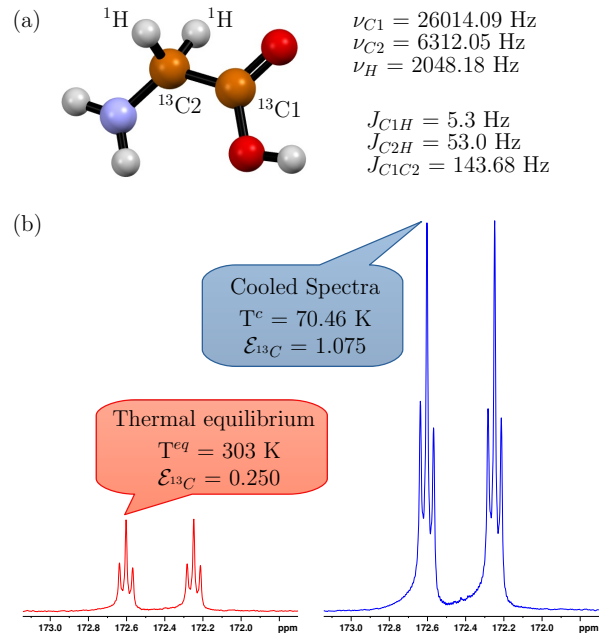


FIG. 4. (a) Molecular structure of  $^{13}\text{C}_2$ -labeled glycine with the  $^{13}\text{C}1$ ,  $^{13}\text{C}2$  and  $^1\text{H}$  spins, encoded as the first, second and third qubit, respectively. The offset rotation frequency for each spin and scalar coupling strengths are listed alongside. (b) The  $^{13}\text{C}$  spectrum (red) on the left was recorded at thermal equilibrium while the spectrum (blue) on the right is the enhanced polarization spectrum recorded after algorithmic cooling of both the  $^{13}\text{C}$  spins. The corresponding polarizations and spin temperatures are annotated.

#### Spin temperature after several TSAC cycles:

The  $^{13}\text{C}$  spectra at thermal equilibrium and after implementation of ten rounds of the TSAC cooling procedure are shown in Fig. 4(b), with ‘hot’ thermal equilibrium spectra shown in red and the algorithmically cooled spectra in blue, plotted to the same scale. The  $^{13}\text{C}$  spectra obtained after algorithmic cooling using the TSAC method show a considerable increase in spin polarization ( $\approx 4.3$  times), with peak intensities being much higher than those obtained at thermal equilibrium. The population of an energy level (and hence the polarization bias) is directly proportional to the area under the corresponding resonance peak and was computed via integration. The theoretical value of maximum achievable  $^{13}\text{C}$  polarization (*Shannon bound*) for the  $^{13}\text{C}_2$ -labeled glycine system computed from Eq. (6) is given by:

$$IC_{\text{eq}} = 17.84 \frac{\epsilon_{\text{eq}}^2}{\ln 4} = \frac{\epsilon_{\text{max}}^2}{\ln 4} \quad (12)$$

$$\Rightarrow \epsilon_{\text{max}} = 4.224 \epsilon_{\text{eq}}$$

After ten rounds of TSAC cooling, we were able to experi-

mentally achieve a final polarization of  $\approx 4.3$  for the  $^{13}\text{C1}$  spin, and were clearly able to surpass the *Shannon bound* for this system. The final spin temperatures attained by the target  $^{13}\text{C1}$  spin, the second  $^{13}\text{C2}$  spin and the reset spin in the  $^{13}\text{C}_2$ -labeled glycine system are tabulated in Table I. It can be seen that the target spin has been substantially cooled down to  $\approx 71$  K. The buildup of  $^{13}\text{C1}$  spin polarization after implementation of every cycle of TSAC cooling is shown in Fig. 5, and saturation of the polarization enhancement is attained after four cycles of TSAC cooling.

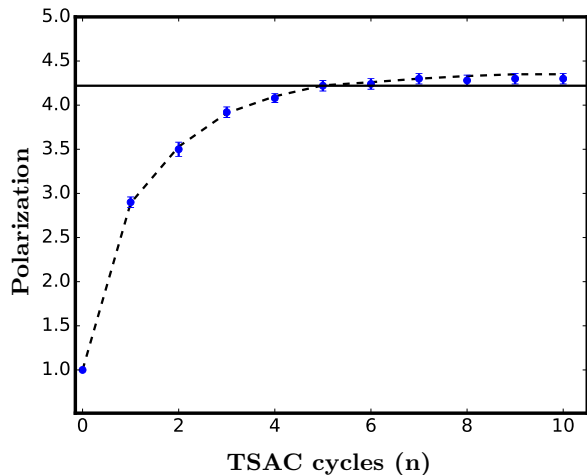


FIG. 5. Polarization of  $^{13}\text{C1}$  spin versus number of cycles ( $n$ ) of TSAC algorithmic cooling implemented on the  $^{13}\text{C}_2$ -labeled glycine system. Theoretically expected and experimentally obtained values are depicted by a black dashed line and blue dots, respectively. The solid black line denotes the *Shannon bound* for maximum achievable polarization.

Spin	Initial Polarization ( $\epsilon_1$ )	Final Polarization ( $\epsilon_2$ )	T(K)
C1	0.25	1.075	70.46
C2	0.25	0.687	110.26
H	1	0.248	1221.77

TABLE I. Initial and final spin polarizations ( $\epsilon_1, \epsilon_2$ ) and final spin temperature (T(K)) attained by each spin in the three-spin  $^{13}\text{C}_2$ -labeled glycine system, after ten rounds of algorithmic cooling.

### Magnetization trajectories during compression unitary implementation:

The plots of individual spin magnetizations of the  $^{13}\text{C}_2$ -labeled glycine system at the end of implementation of each gate in the quantum circuit of the TSAC algorithm are shown in Fig. 9(a). The way entropy compression proceeds after each gate can be visualized from these magnetization plots, with the magnetization being plotted on the  $y$ -axis, and the gate number being denoted along the  $x$ -axis; gate number 1, 2, 3, 4, 5, 6, 7 and 8 corresponds to a NOT, CNOT, Toffoli, Toffoli, NOT, Toffoli, CNOT and NOT gate, respectively (Fig. 2(a)). The

first three gates comprise the right shift operator, after implementation of which, the entropy of the  $^{13}\text{C1}$  spin is decreased, that of the  $^{13}\text{C2}$  spin is maximized and that of the  $^1\text{H}$  spin remains the same. As seen from Fig. 9(a), the sixth gate which is a Toffoli gate has achieved entropy compression and complete increase of  $^{13}\text{C1}$  polarization. The subsequent gates manipulate the  $^{13}\text{C2}$  magnetization and invert the  $^1\text{H}$  magnetization; the protocol could have been truncated at the seventh gate, which would have reduced the circuit complexity.

### C. Experimentally Cooling the $^{15}\text{N}$ Spin

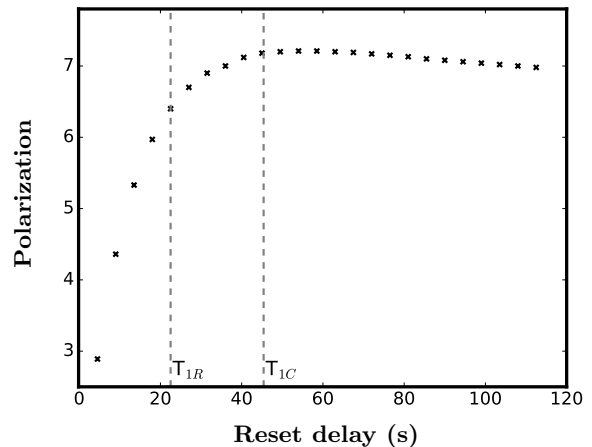


FIG. 6. Simulation of  $^{15}\text{N}$  spin polarization as a function of the TSAC reset delay for the  $^{13}\text{C}$ - $^{15}\text{N}$ -labeled formamide system;  $T_{1R}$  and  $T_{1C}$  mark the  $T_1$  relaxation times of the  $^1\text{H}$  reset spin and the  $^{15}\text{N}$  computation spin, respectively.

We were interested in exploring the efficiency of the TSAC algorithm on  $^{15}\text{N}$  spins, due to their low initial polarizations at thermal equilibrium ( $\approx 1/10$ th that of the  $^1\text{H}$  spin) as well as long  $T_1$  relaxation rates, which makes them attractive target spins for cooling. Hence  $^{15}\text{N}$  was chosen as the main target spin to be cooled in the  $^{13}\text{C}$ - $^{15}\text{N}$ -labeled formamide system and  $^1\text{H}$  was chosen as the reset spin. This system also contains a  $^{13}\text{C}$  spin which can also potentially be cooled down by the TSAC protocol. The reset spin relaxes much faster as compared to the other spins and hence can be made to equilibrate quickly with the heat-bath while the target spin remain relatively isolated from the heat-bath.

#### Optimizing the TSAC reset delay:

In order to optimize the reset delay at the end of the compression unitary implementation in the TSAC protocol, we simulated the change in  $^{15}\text{N}$  spin polarization as a function of the reset delay. The TSAC reset delay was varied from  $0.2 \cdot T_1$  to  $5 \cdot T_1$  for the reset spin (Eq. (11)) and as can be seen from Fig. 6, maximum  $^{15}\text{N}$  polarization was obtained for a reset delay of  $\approx 2.5 T_1$ . We hence set the value of the reset delay to this optimal value and

performed multiple rounds of TSAC cooling.

### Spin temperature after several TSAC cycles:

The  $^{15}\text{N}$  spectra at thermal equilibrium (spectra plotted in red color) and after implementation of the TSAC cooling procedure (spectra plotted in blue color) are shown in Fig. 7(b). A substantial increase in polarization of the  $^{15}\text{N}$  was achieved after TSAC cooling ( $\approx 5.95$  times). As seen from the spectra in Fig. 7(b), the spectral peaks at the extreme positions in the thermal equilibrium spectra are barely visible, while after algorithmic cooling their signal-to-noise ratio has been significantly increased. The theoretical value of maximum achievable  $^{15}\text{N}$  polarization (*Shannon bound*) for the  $^{13}\text{C}$ - $^{15}\text{N}$ -labeled formamide system computed from Eq. (6) is given by:

$$IC_{\text{eq}} = 104.56 \frac{\epsilon_{\text{eq}}^2}{\ln 4} = \frac{\epsilon_{\text{max}}^2}{\ln 4} \quad (13)$$

$$\Rightarrow \epsilon_{\text{max}} = 10.22\epsilon_{\text{eq}}$$

After six rounds of TSAC cooling, we were able to experimentally achieve a final  $^{15}\text{N}$  polarization of 0.595, and were not able to surpass the *Shannon bound* for this system. The final spin temperatures attained by all the three spins in the  $^{13}\text{C}$ - $^{15}\text{N}$ -labeled formamide system are tabulated in Table II. While the  $^{15}\text{N}$  spin shows substantial cooling down to  $\approx 51$  K, it is noteworthy that the  $^{13}\text{C}$  spin has also been cooled down to  $\approx 187$  K. The buildup of  $^{15}\text{N}$  spin polarization after implementation of every cycle of TSAC cooling is shown in Fig. 8, and saturation of the polarization enhancement is attained after three cycles of TSAC cooling.

Spin	Initial Polarization ( $\epsilon_1$ )	Final Polarization ( $\epsilon_1$ )	T(K)
N	0.101	0.595	51.43
C	0.251	0.406	187.32
H	1	-0.187	1620.32

TABLE II. Initial and final spin polarizations ( $\epsilon_1$ ,  $\epsilon_2$ ) and final spin temperature (T(K)) attained by each spin in the three-spin  $^{13}\text{C}$ - $^{15}\text{N}$ -labeled formamide system, after several rounds of algorithmic cooling.

	H	C2	C1 <sup>hot</sup>	C1 <sup>cold</sup>
T <sub>1</sub>	1.57±0.01	3.23±0.03	20.4±0.57	18.6±0.4
T <sub>2</sub>	1.0±0.01	1.16±0.02	1.53±0.01	1.4±0.01

TABLE III. Measured relaxation times (in seconds) of all the spins in the three-spin  $^{13}\text{C}_2$ -labeled glycine system, including the target spin at thermal equilibrium (C1<sup>hot</sup>) and after algorithmic cooling (C1<sup>cold</sup>).

### Magnetization trajectories during compression unitary implementation:

The plots of individual spin magnetizations of the  $^{13}\text{C}$ - $^{15}\text{N}$ -labeled formamide system at the end of the implementation of each quantum gate in the quantum circuit of the TSAC algorithm are shown in Fig. 9(b). The first three gates comprise the right shift operator, after implementation of which, the entropy of the  $^{15}\text{N}$  spin is

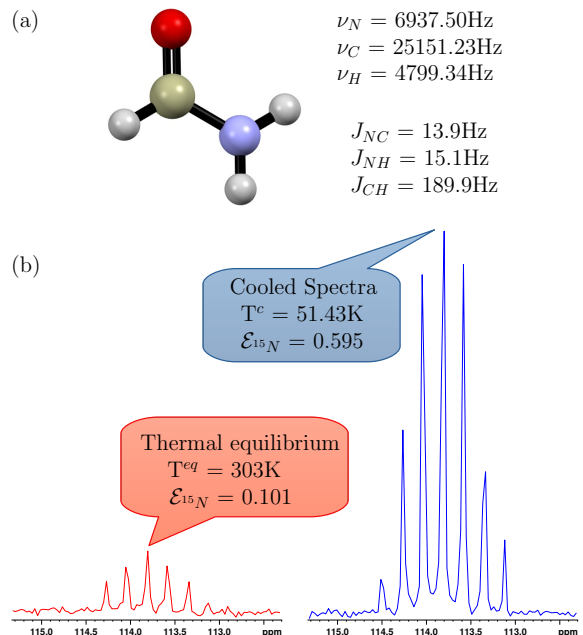


FIG. 7. (a) Molecular structure of  $^{13}\text{C}$ - $^{15}\text{N}$ -labeled formamide, with the  $^{15}\text{N}$ ,  $^{13}\text{C}$  and  $^1\text{H}$  spins encoded as the first, second and third qubit, respectively. The offset rotation frequency for each spin and the scalar J coupling strengths are listed alongside. (b) The  $^{15}\text{N}$  NMR spectrum (red) on the left was recorded at thermal equilibrium while the spectrum (blue) on the right is the enhanced polarization spectrum recorded after algorithmic cooling of the  $^{15}\text{N}$  spin. The corresponding polarizations and spin temperatures are annotated.

	H	C	N <sup>hot</sup>	N <sup>cold</sup>
T <sub>1</sub>	22.5±0.675	30.40±1.55	45.35±2.25	50.67±3.39
T <sub>2</sub>	1.15±0.16	1.33±0.07	0.095±0.009	0.115±0.01

TABLE IV. Measured relaxation times (in seconds) of all the spins in the three-spin  $^{13}\text{C}$ - $^{15}\text{N}$ -labeled formamide system, including the target spin at thermal equilibrium (N<sup>hot</sup>) and after algorithmic cooling (N<sup>cold</sup>).

decreased, that of the  $^{13}\text{C}$  spin is maximized and that of the  $^1\text{H}$  spin remains the same. Hence at this stage, the magnetizations of the  $^{15}\text{N}$ ,  $^{13}\text{C}$  and  $^1\text{H}$  spins are halved, zeroed and inverted, respectively. The sixth gate in the circuit, which is a Toffoli gate with control on the  $^1\text{H}$  and  $^{13}\text{C}$  spins and target on the  $^{15}\text{N}$  spin has decreased the entropy of the  $^{15}\text{N}$  spin and correspondingly increased its polarization to its final experimental polarization. The final CNOT and NOT gates act to decrease the entropy of the  $^{13}\text{C}$  spin and invert the magnetization of the  $^1\text{H}$  spin.

In summary, the TSAC cooling protocol performs very well in cooling spins with low initial polarizations such as  $^{13}\text{C}$  and  $^{15}\text{N}$  spins. The protocol is robust and experimentally feasible. While maximum possible cooling was not achieved experimentally for the  $^{15}\text{N}$  spin, this could be attributed to several factors including decoherence, rf

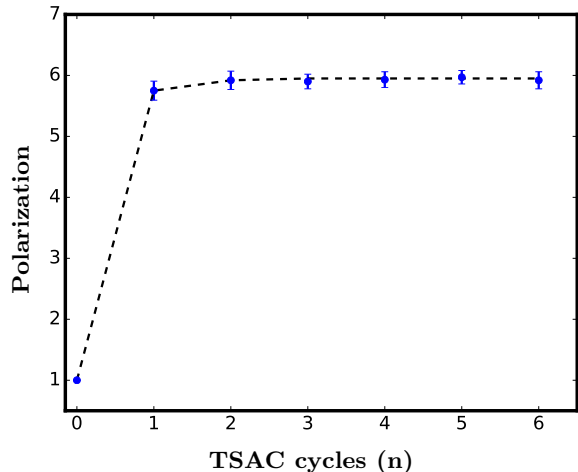


FIG. 8. Polarization of the  $^{15}\text{N}$  spin versus number of cycles ( $n$ ) of TSAC algorithmic cooling implemented on the  $^{13}\text{C}$ - $^{15}\text{N}$ -labeled formamide system. Theoretically expected and experimentally obtained values are depicted by a black dashed line and blue dots, respectively.

inhomogeneities and errors in the calibration of rf pulse parameters. The measured  $T_1$  relaxation times (in seconds) of all the spins in the  $^{13}\text{C}_2$ -labeled glycine system and in the  $^{13}\text{C}$ - $^{15}\text{N}$ -labeled formamide system are tabulated in Tables III and IV, respectively. The relaxation dynamics of the algorithmically cooled spins does not change appreciably after implementation of the TSAC protocol, implying that these systems retain their good dynamics properties, which are important for quantum computing. The gap between the numerically computed upper bounds on the achievable polarizations for perfect TSAC conditions and the experimentally achieved polarizations suggests that cooling can be enhanced in systems with favorable relaxation properties by implementing several cycles of the TSAC protocol.

#### IV. CONCLUSIONS

A major drawback of all standard HBAC protocols is that the operations for implementing compression are rather complex, change after every iteration, and hence require knowledge of the state in each iteration. A new HBAC protocol was designed which reaches the cooling limit using a fixed state-independent operation as the compression step, TSAC method. We used the TSAC method to purify selected target qubits in a system containing computational and reset qubits. We designed an optimal circuit decomposition of the compression unitary used in the protocol in terms of standard CNOT, Toffoli and NOT gates which are experimentally viable to implement. Using an NMR quantum processor, we experimentally demonstrated the efficacy of the two-sort algorithmic cooling method in two different systems containing a

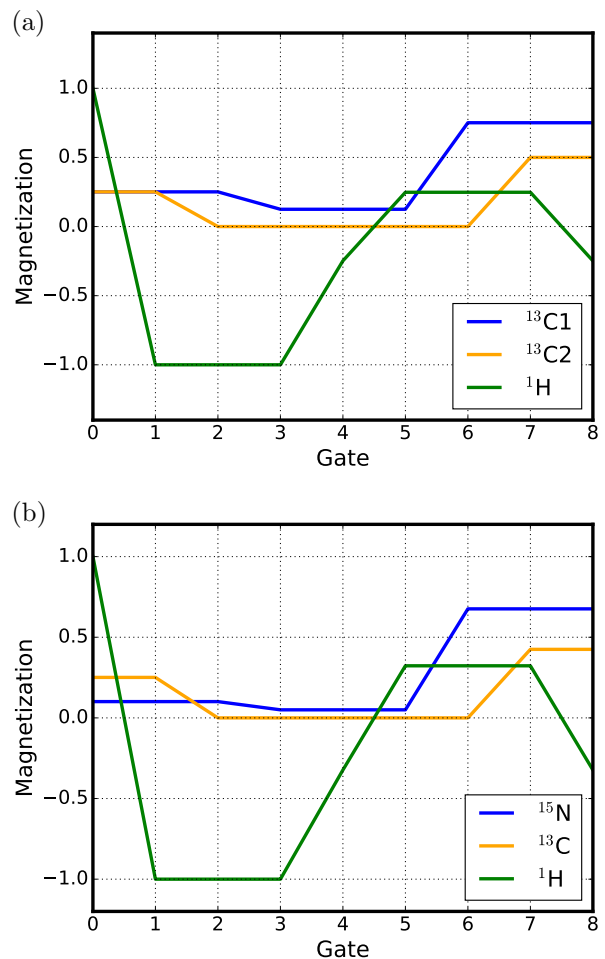


FIG. 9. Plots of individual spin magnetizations after implementation of each quantum gate in the circuit of the compression unitary  $U_{TS}$  for the (a)  $^{13}\text{C}_2$ -labeled glycine system and the (b)  $^{13}\text{C}$ - $^{15}\text{N}$ -labeled formamide system. The gate number is indicated on the  $x$ -axis.

target  $^{13}\text{C}$  and  $^{15}\text{N}$  spin. We obtained large polarization enhancements for both spins, which implies an appreciable decrease in the corresponding spin temperatures. We achieved significant cooling of the  $^{15}\text{N}$  spin, with a polarization enhancement by a factor of  $\approx 5.95$  which implies cooling down to a temperature  $\approx 51\text{ K}$ . Since  $^{15}\text{N}$  has a very low polarization at room temperatures, our work has important implications for enhancing the signal-to-noise ratios, thereby reducing experimental acquisition times for  $^{15}\text{N}$ -labeled biomolecules such as peptides and proteins.

Since heat-bath algorithmic cooling methods reduce the spin entropy and achieve spin cooling (and enhanced spin polarization) without the need for physical cooling of the system, they are safe and robust and have immense applications for *in vivo* NMR spectroscopy of slow metabolic processes. The two-sort heat-bath algorithmic cooling method is general and experimentally feasible, and can be used to cool qubits in other quantum process-

ing devices as well. Future work in this direction includes using the two-sort algorithm to enhance cooling of target qubits in larger-qubit registers and to investigate the performance of this algorithm and the attainable cooling limit in the presence of realistic noise.

## ACKNOWLEDGMENTS

All experiments were performed on a Bruker Avance-III 600 MHz NMR spectrometer at the NMR Research Facility at IISER Mohali. K. S. thanks Akshay, Dileep and Mamta for useful discussions. K. S. acknowledges financial support from the Prime Minister's Research Fellowship(PMRF) scheme of the Government of India. Arvind acknowledges funding from the Department of Science and Technology (DST), India, Grant No:DST/ICPS/QuST/Theme-1/2019/Q-68. K.D. acknowledges funding from the Department of Science and Technology (DST), India, Grant No:DST/ICPS/QuST/Theme-2/2019/Q-74.

- 
- [1] S. Raeisi, M. Kieferová, and M. Mosca, *Phys. Rev. Lett.* **122**, 220501 (2019).
- [2] M. A. Nielsen and I. L. Chuang, *Quantum Computation and Quantum Information* (Cambridge University Press, 2010).
- [3] P. W. Shor, *SIAM Journal on Computing* **26**, 1484 (1997).
- [4] A. W. Harrow, A. Hassidim, and S. Lloyd, *Phys. Rev. Lett.* **103**, 150502 (2009).
- [5] T. Wang, R. Ghobadi, S. Raeisi, and C. Simon, *Phys. Rev. A* **88**, 062114 (2013).
- [6] J. Preskill, *Proceedings of the Royal Society of London. Series A: Mathematical, Physical and Engineering Sciences* **454**, 385 (1998).
- [7] D. G. Cory, R. Laflamme, E. Knill, L. Viola, T. F. Havel, N. Boulant, G. Boutis, E. Fortunato, S. Lloyd, R. Martinez, C. Negrevergne, M. Pravia, Y. Sharf, G. Teklemariam, Y. S. Weinstein, and W. H. Zurek, *Fortschritte der Physik* **48**, 875 (2000).
- [8] L. M. K. Vandersypen and I. L. Chuang, *Rev. Mod. Phys.* **76**, 1037 (2005).
- [9] K. Dorai, T. S. Mahesh, Arvind, and A. Kumar, *Current Science* **79**, 1447 (2000).
- [10] D. P. Divincenzo, *Fortschritte der Physik* **48**, 771 (2000).
- [11] N. Linden and S. Popescu, *Phys. Rev. Lett.* **87**, 047901 (2001).
- [12] L. J. Schulman and U. V. Vazirani, in *IN 31ST STOC* (1999) pp. 322–329.
- [13] J. H. Ardenkjaer-Larsen, B. Fridlund, A. Gram, G. Hansson, L. Hansson, M. H. Lerche, R. Servin, M. Thaning, and K. Golman, *Proceedings of the National Academy of Sciences* **100**, 10158 (2003).
- [14] P. Bhattacharya, K. Harris, A. P. Lin, M. Mansson, V. A. Norton, W. H. Perman, D. P. Weitekamp, and B. D. Ross, *MAGMA* **18**, 245 (2005).
- [15] A.-M. Oros and N. J. Shah, *Physics in Medicine and Biology* **49**, R105 (2004).
- [16] T. M. Cover and J. A. Thomas, *Elements of Information Theory* (Wiley-Interscience, 2006).
- [17] P. O. Boykin, T. Mor, V. Roychowdhury, F. Vatan, and R. Vrijen, *Proceedings of the National Academy of Sciences* **99**, 3388 (2002).
- [18] J. M. Fernandez, S. Lloyd, T. Mor, and V. Roychowdhury, *International Journal of Quantum Information* **02**, 461 (2004).
- [19] L. J. Schulman, T. Mor, and Y. Weinstein, *SIAM Journal on Computing* **36**, 1729 (2007).
- [20] L. J. Schulman, T. Mor, and Y. Weinstein, *Phys. Rev. Lett.* **94**, 120501 (2005).
- [21] Y. Elias, T. Mor, and Y. Weinstein, *Phys. Rev. A* **83**, 042340 (2011).
- [22] S. Raeisi and M. Mosca, *Phys. Rev. Lett.* **114**, 100404 (2015).
- [23] N. A. Rodríguez-Briones and R. Laflamme, *Phys. Rev. Lett.* **116**, 170501 (2016).
- [24] Á. M. Alhambra, M. Lostaglio, and C. Perry, *Quantum* **3**, 188 (2019).
- [25] S. Raeisi, *Phys. Rev. A* **103**, 062424 (2021).
- [26] Z. Farahmand, R. Aghaei Saem, and S. Raeisi, *Phys. Rev. A* **105**, 022418 (2022).
- [27] J. Baugh, O. Moussa, C. A. Ryan, A. Nayak, and R. Laflamme, *Nature* **438**, 470 (2005).
- [28] J. M. Fernandez, T. Mor, and Y. Weinstein, *International Journal of Quantum Information* **03**, 281 (2005).
- [29] Y. Elias, H. Gilboa, T. Mor, and Y. Weinstein, *Chemical Physics Letters* **517**, 126 (2011).
- [30] G. Brassard, Y. Elias, J. M. Fernandez, H. Gilboa, J. A. Jones, T. Mor, Y. Weinstein, and L. Xiao, *The European Physical Journal Plus* **129**, 266 (2014).
- [31] Y. Atia, Y. Elias, T. Mor, and Y. Weinstein, *Phys. Rev. A* **93**, 012325 (2016).
- [32] V. R. Pande, G. Bhole, D. Khurana, and T. S. Mahesh, *Phys. Rev. A* **96**, 012330 (2017).
- [33] C. A. Ryan, O. Moussa, J. Baugh, and R. Laflamme, *Phys. Rev. Lett.* **100**, 140501 (2008).
- [34] E. Köse, S. m. c. Çakmak, A. Gençten, I. K. Kominis, and O. E. Müstecaplıoğlu, *Phys. Rev. E* **100**, 012109 (2019).
- [35] N. A. Rodríguez-Briones, J. Li, X. Peng, T. Mor, Y. Weinstein, and R. Laflamme, *New Journal of Physics* **19**, 113047 (2017).
- [36] S. Zaiser, C. T. Cheung, S. Yang, D. B. R. Dasari, S. Raeisi, and J. Wrachtrup, *npj Quantum Information* **7**, 92 (2021).
- [37] K. Dorai and D. Suter, *International Journal of Quantum Information* **03**, 413 (2005).
- [38] O. W. Sørensen, *Progress in Nuclear Magnetic Resonance Spectroscopy* **21**, 503 (1989).

- [39] A. Barenco, C. H. Bennett, R. Cleve, D. P. DiVincenzo, N. Margolus, P. Shor, T. Sleator, J. A. Smolin, and H. Weinfurter, *Phys. Rev. A* **52**, 3457 (1995).
- [40] I. S. Oliveira, T. J. Bonagamba, R. S. Sarthour, J. C. C. Freitas, and E. R. deAzevedo, *NMR quantum information processing* (Elsevier Science B.V., Amsterdam, 2007).
- [41] D. Das, S. Dogra, K. Dorai, and Arvind, *Phys. Rev. A* **92**, 022307 (2015).
- [42] H. Singh, Arvind, and K. Dorai, *Phys. Rev. A* **97**, 022302 (2018).
- [43] A. Singh, H. Singh, K. Dorai, and Arvind, *Phys. Rev. A* **98**, 032301 (2018).